High-Pressure Phase Equilibria for Polypropylene−Hydrocarbon Systems

J. Vladimir Oliveira,* C. Dariva, and J. C. Pinto

Chemical Engineering Program, PEQ/COPPE/UFRJ, Rio de Janeiro, Brazil 21945-970

The objective of this work is to provide new high-pressure phase equilibrium data for a commercial isotactic polypropylene grade with some hydrocarbon solvents (propane, propylene, *n*-butane, and 1-butene). The experiments were performed in a high-pressure, variable-volume view cell in the temperature range of 80−150 °C and in polymer composition from 0.3 to 10 wt %. Phase transitions were visually recorded as cloud points and identified as liquid−liquid, vapor−liquid, and vapor−liquid−liquid. It was experimentally observed that the use of paraffins, at the same temperature and composition, led to a decrease in the pressure transition when compared to the olefins (with the same chain length), thus increasing the one-phase region. The $P-T$ diagram for these systems were constructed, affording the location of the lower critical solution temperature curves as well as the lower critical equilibrium pressures. Experimental tests were also carried out for solutions containing toluene as the cosolvent, and it was observed that the increase of toluene concentrations leads to the decrease of the two-phase region.

Introduction

The thermodynamics of polymer systems plays an important role in most polymerization processes and very often is a key factor for polymer production, processing, and material development. For instance, the proper understanding of thermodynamic equilibrium of polymer solutions allows the online monitoring and control of polymerization reactions,[1] which would be impossible otherwise. Besides, because most polymerizations are carried out in heterogeneous media, the understanding of monomer partitioning among the various phases is fundamental for proper kinetic interpretation and the design of molecular weight distributions (MWDs).[2,3] It is also well-known that the thermodynamic behavior of polymer solutions exerts a major influence upon the morphology of the final polymer powder obtained, which has led to the development of interesting studies about the precipitation conditions in dispersion polymerizations at low and high pressures.[4−6] Recently, much attention has been concentrated upon the formation of particle morphology and particle size distributions when polymerization is performed at supercritical conditions.[7] Several applications for the polymer microparticles generated at supercritical conditions can be envisaged, such as the development of new packings for chromatography, preparation of adsorbents, production of new catalyst supports, etc.[8] Among the several process variables that influence the characteristics of the precipitated particles, knowledge about phase the behavior of the systems under investigation is of primary importance for any microparticle formation technique.

The phase behavior of polymer solutions depends strongly on the energetic interactions and on the size differences between polymer and solvent molecules. At temperatures close to the solvent critical point, polymer precipitates because of the much larger thermal expansion coefficient of the solvent (the free-volume effect), when compared to that of the polymer. This type of phase split is known as the lower critical solution temperature (LCST) phase transition and is characterized by an increase in the pressure with temperature, i.e., $(\partial P/\partial T)_x > 0$, because the hydrostatic pressure decreases the free-volume differences between the polymer and solvent and hence makes them more compatible. At lower temperatures, differences of energetic interactions between polymer and solvent molecules may lead to limited polymer solubility and phase split, known as the upper critical solution temperature (UCST) phase transition.[9−11] Sometimes, the UCST may be located at such low temperatures that the solution may intersect the polymer solidification boundary before phase separation occurs.[12]

Production of polyolefins is a multibillion dollar business, responsible for the production of more than 80 million metric tons of polymer resins and moving approximately 50 billion U.S. dollars worldwide/year.[13] The vast majority of the polyolefin production is concentrated on the production of polyethylenes (PE), polypropylenes (PP), and PE−PP copolymers and blends. Because of the enormous economic importance of the polyolefin business, the thermodynamic study of polyolefin systems has received a lot of attention in the open literature.

The most extensively studied polymer systems over the past 30 years certainly are solutions of PE in hydrocarbon solvents. Folie and Radosz[11] reviewed the phase equilibria of ethylene homopolymer and copolymer systems in supercritical solutions. Cloud-point data for other polyolefin systems have also been reported in the literature.[14−19] However, despite the economic importance of the PP market and the rapidly growing installed production capacity of PP plants, investigations about the high-pressure phase equilibrium of PP solutions have hardly been presented in the literature. Indeed, just a few experimental data, like those from Whaley et al.,[20] who studied the phase equilibria of the PP−propane system, have been reported. Therefore, the study of propylene polymerizations and PP particle

* To whom correspondence should be addressed. E-mail: vladimir@peq.coppe.ufrj.br. Fax: +55-21-5907135.

10.1021/ie990895s CCC: $19.00
Published on Web 11/02/2000

formation at high pressures is seriously impaired by the lack of data.

In this context, the main objective of this work is to provide new high-pressure phase equilibrium data for a commercial PP grade in some usual hydrocarbon solvents (propane, *n*-butane, propylene, and 1-butene) used in the olefin industry, in a wide range of temperatures and pressures and for polymer compositions ranging from 0.3 to 10 wt %. Though phase equilibrium data for well-characterized, almost monodisperse polymer samples may be much more useful for a theoretical thermodynamic analysis, the use of polydisperse PP samples, as received from industry, is of great interest for practical purposes. Special attention is given here to the identification of the LCST curves and to the influence of toluene upon the thermodynamic behavior of PP solutions. Toluene was chosen as the cosolvent because of its use very often for related kinetic studies and as a means to suspension storage.

Experimental Section

Materials. The solvents used in this work were propylene (C.P. grade, 99.5% minimum purity), propane (analytical grade, 99.5% minimum purity), 1-butene (C.P. grade, 99.0% minimum purity), and *n*-butane (C.P. grade, 99.5% minimum purity). All solvents were purchased from AGA S.A.

Commercial PP was kindly supplied by Polibrasil Resinas S.A. PP samples were produced with supported high-activity Ziegler−Natta catalysts. The average molecular weight ($M_w = 245\,000$) and polydispersity index ($M_w/M_n = 5.01$) were determined through gel permeation chromatography (GPC) in a Waters 150CV chromatograph, equipped with four Ultrastyragel separation columns (10^3, 10^4, 10^5, and 10^6 Å) from Waters. Polymer samples were dissolved in 1,2,4-trichlorobenzene (TCB), and measurements were performed at 140 °C. Polystyrene standards from Polymer were used to calibrate the GPC. The degree of isotacticity (92%) was measured as the molar fraction of isotactic diads through ^{13}C NMR analysis in a Varian Inova 300 equipment, at frequencies of 75.4 MHz. The time interval used for analysis was equal to 10 s. Polymer samples were dissolved in TCB, and measurements were performed at 95 °C. Differential scanning calorimetry (DSC) analysis (Pelkin Elmer DSC 500) of PP samples indicates that the melting temperature (T_m) is around 159.3 °C.

Apparatus. Phase equilibrium experiments (cloud points) were performed in a high-pressure, variable-volume view cell. A schematic diagram of the apparatus is presented in Figure 1. The apparatus consists basically of a view cell with three sapphire windows for visual observations, an absolute pressure transducer (Smar LD 301), with a precision of ±0.012 MPa, a portable programmer (Smar HT 201) for the pressure data acquisition, and a syringe pump (ISCO 260D). The equilibrium cell has a maximum internal volume of 28 cm^3 and contains a movable piston, which permits pressure control inside the cell. Phase transitions were recorded visually through manipulation of the pressure, using the syringe pump and the solvent (propylene, propane, 1-butene, or *n*-butane, depending on the system under study) as the pressurizing fluid. The cell is equipped with an electrical heater and a proportional−integral−differential temperature controller (Dextron DTS4). The controller is connected to a thermocouple, which is in direct contact with the fluid mixture inside the cell body. This arrangement provided a temperature control with a precision of 0.5 °C. The experimental apparatus, as hydrostatically tested up to 350 bar at room temperature, was employed to conduct the experiments up to 270 bar and 150 °C.

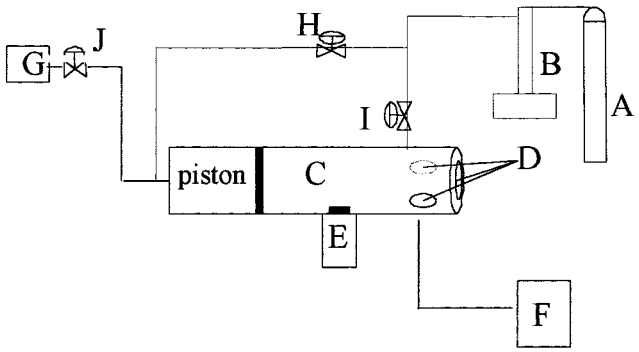

Figure 1. Schematic diagram of the phase equilibrium apparatus: A, CO_2 cylinder; B, syringe pump; C, equilibrium cell; D, sapphire windows; E, magnetic stirrer; F, white light source; G, pressure transducer; H, ball valve; I, micrometering valve; J, relief valve.

Procedure. Depending on the desired global composition, an amount of polymer was weighed on a high-precision scale (Ohaus Analytical Standard, with 0.0001 g accuracy) and loaded into the cell. Then, the cell and all lines were flushed with low-pressure gas to remove residual air. Afterward, the solvent was pumped into the cell in order to reach the preestablished global composition. The amount of solvent charged was monitored by the change in the total mass of the transfer vessel of the pump. Then, the cell content was kept at continuous agitation with the help of a magnetic stirrer and a Teflon-coated stirring bar.

After the desired temperature was reached, the cell pressure was increased until observation of a single phase. At this point, the cell pressure was decreased slowly until incipient formation of a new phase. The equilibrium pressure was then recorded, after repetition of the experimental procedure at least four times, leading to an average reproducibility of 0.70 bar. After completion of the test at a given temperature, the cell temperature was stabilized at a new value and the experimental procedure was repeated.

The reliability of experimental measurements with the present apparatus has been confirmed[21] by studying the system ethanol−carbon dioxide and comparing bubble point data obtained with the view cell just described with data published in the open literature.[22−24]

Results and Discussion

Table 1 shows the phase equilibrium data obtained for the system PP−*n*-butane. Cloud-point pressures were determined at different temperatures for several polymer weight compositions. At temperatures of around 85 °C, the appearance of a solid phase was observed for all compositions. These transitions were characterized by the turbidity of the solid suspension, which did not disappear upon increasing the cell pressure up to 270 bar. (It is assumed here that the crystallization boundary has been intersected whenever the increase of the cell pressure up to 270 bar does not allow the restoration of the one-phase region.)

Figure 2 presents the $P-x$ diagram [liquid (L) to LL transition] for some selected temperatures, where it can be observed that the cloud-point isotherms are relatively

Table 1. Experimental Results for the PP−*n*-Butane System[a]

polym wt %	*T* [°C]	*P* [bar]	equilibrium type	polym wt %	*T* [°C]	*P* [bar]	equilibrium type
0.30	150	106.3	LL	1.00	150	113.4	LL
	140	88.6	LL		140	95.7	LL
	140	33.5	VLL		140	33.4	VLL
	130	69.8	LL		130	77.4	LL
	130	28.5	VLL		130	28.4	VLL
	120	51.6	LL		120	58.9	LL
	120	24.4	VLL		120	24.4	VLL
	110	31.7	LL		110	40.9	LL
	110	21.1	VLL		110	21.4	VLL
	100	16.7	VL		100	22.5	LL
	95	15.2	VL		100	17.0	VLL
	90	13.9	VL		95	16.7	VL
	85	12.4	VL		90	15.5	VL
0.69	150	112.4	LL		85	13.6	VL → S
	140	95.0	LL	2.98	150	114.2	LL
	140	33.6	VLL		150	39.2	VLL
	130	77.4	LL		140	96.0	LL
	130	28.4	VLL		140	33.6	VLL
	120	58.4	LL		130	77.9	LL
	120	24.6	VLL		130	29.2	VLL
	110	38.9	LL		120	60.5	LL
	110	21.1	VLL		120	25.3	VLL
	100	21.5	LL		110	42.2	LL
	100	17.0	VLL		110	21.5	VLL
	95	16.0	VL		100	22.0	LL
	90	15.0	VL		100	17.2	VLL
	85	13.6	VL → S*		95	17.0	VL
					90	15.7	VL
					85	13.7	VL → S
4.96	150	114.8	LL	7.42	150	112.1	LL
	150	39.5	VLL		140	95.4	LL
	140	98.5	LL		130	78.1	LL
	140	33.7	VLL		120	60.0	LL
	130	82.9	LL		110	41.2	LL
	130	28.7	VLL		100	21.9	LL
	120	64.8	LL		90	14.7	VL
	120	24.8	VLL		85	13.3	VL → S
	110	45.1	LL	9.92	150	109.0	LL
	110	21.0	VLL		140	93.9	LL
	100	24.5	LL		130	77.0	LL
	100	17.1	VLL		120	57.4	LL
	95	17.2	VL		110	38.1	LL
	90	15.6	VL		100	21.3	LL
	85	13.9	VL → S		95	16.0	VL
					90	14.5	VL
					85	13.1	VL → S

[a] → S* is the appearance of a solid phase.

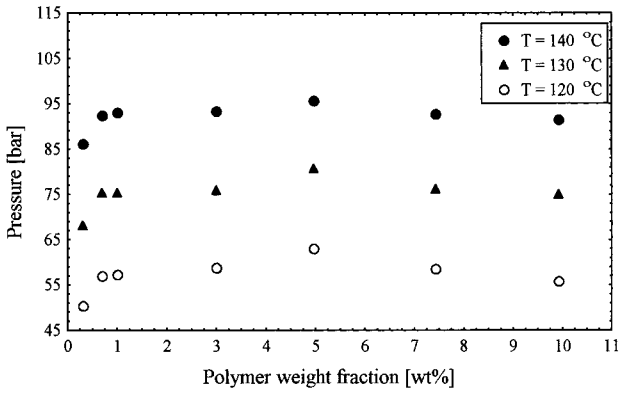

Figure 2. Experimental PP cloud-point behavior in *n*-butane. Transition from L to LL. *P*−*x* diagram.

flat for polymer compositions greater than 0.70 wt %. The occurrence of a plateau for phase transition diagrams of polymer systems has also been observed by other researchers, especially around the critical concentrations.[25] Also, because the solution is, in fact, a

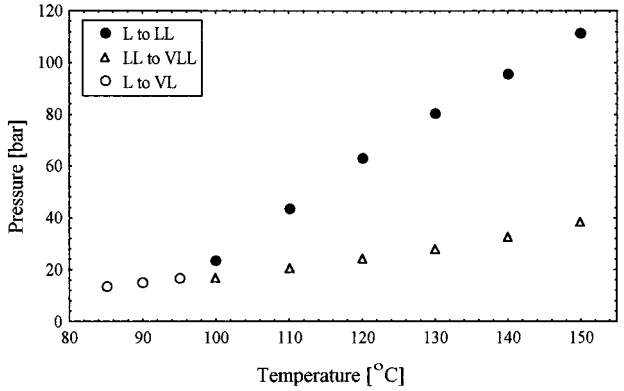

Figure 3. *P*−*T* diagram for PP−*n*-butane at a polymer concentration of 5 wt %.

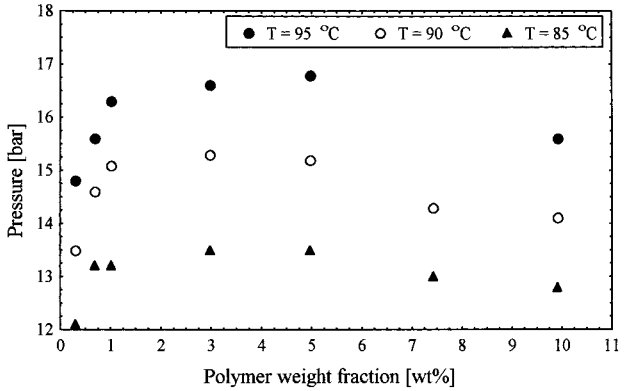

Figure 4. Cloud-point L to VL behavior for the system PP−*n*-butane.

multicomponent system because of the high polydispersity index of the polymer, the identification of cloud points is more complex and thus can possibly lead to the identification of flat isotherms. Critical concentrations (maximum in the *P*−*x* curves) are estimated to be approximately between 3 and 5 wt %, as can be seen in Figure 2. These critical concentration values are coherent with those frequently presented in the literature for polymer−solvent systems (typically around 5 wt %).

Figure 3 presents the *P*−*T* diagram for 5 wt % PP concentration where one can observe the usual LCST phase behavior found for high molecular weight polymer−supercritical fluid solvent systems. The existence of the LCST curve for polymer−subcritical and −supercritical solvent systems has been explained in terms of the difference of thermal expansion coefficients between the polymer and solvent species.[11,16,25] The VLL and VL phase split curves (where V is vapor) are also plotted in Figure 3. For binary polymer−solvent systems, the three-phase line is very close to the solvent vapor pressure, and the intersection of this curve with the LL and VL curves defines the LCEP of the system at a given composition. At temperatures below this point, phase split from L to VL is observed. The plot of the three-phase VLL experimental data obtained in this work conforms to a line opposite to the region expected for polydisperse polymer−solvent systems. The location of LCEPs as a function of PP composition for these systems can be obtained straightforwardly: 102, 97.5, 97, 97, 95.5, 97, and 98 °C for polymer weight fractions of 0.30, 0.69, 1.00, 2.98, 4.96, 7.42, and 9.92 wt %, respectively.

Figure 4 presents the *P*−*x* diagram for the VL phase separation of the PP/*n*-butane system. Maximum pres-

Table 2. Experimental Results for the PP−1-Butene System

polym wt %	*T* [°C]	*P* [bar]	equilibrium type	polym wt %	*T* [°C]	*P* [bar]	equilibrium type
0.30	150	113.7	LL	2.97	150	132.3	LL
	140	100.7	LL		145	124.1	LL
	130	91.1	LL		140	116.2	LL
	120	73.9	LL		135	106.7	LL
	110	53.1	LL		130	98.3	LL
	100	35.8	LL		125	89.4	LL
	90	15.9	VL → S		120	80.1	LL
0.69	150	127.3	LL		115	69.4	LL
	140	110.4	LL		110	60.8	LL
	130	96.6	LL		105	50.1	LL
	120	78.2	LL		100	40.1	LL
	110	58.9	LL		95	29.0	LL
	100	38.6	LL		90	18.4	LL → S
	90	17.6	VL → S	4.96	150	132.2	LL
0.99	150	129.2	LL		145	124.7	LL
	145	120.2	LL		140	116.1	LL
	140	114.5	LL		135	107.5	LL
	135	106.7	LL		130	99.8	LL
	130	99.2	LL		125	89.5	LL
	125	90.2	LL		120	80.9	LL
	120	80.7	LL		110	61.1	LL
	115	71.4	LL		100	40.5	LL
	110	61.4	LL		90	18.4	LL → S
	105	51.2	LL	7.43	150	133.1	LL
	100	41.1	LL		145	125.9	LL
	95	29.8	LL		140	116.3	LL
	90	18.4	LL → S		135	107.3	LL
	85	14.7	VL → S		130	101.2	LL
9.96	150	129.1	LL		125	89.9	LL
	145	120.3	LL		120	82.1	LL
	140	112.8	LL		110	62.1	LL
	135	106.1	LL		100	42.6	LL
	130	97.2	LL		90	20.3	LL → S
	125	88.2	LL				
	120	77.5	LL				
	110	58.8	LL				
	100	38.9	LL				
	90	18.9	LL → S				

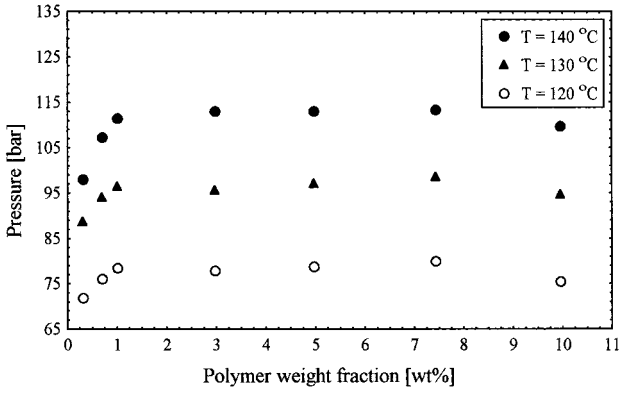

Figure 5. Experimental PP cloud-point behavior in 1-butene. Transition from L to LL. *P*−*x* diagram.

sure values can be observed around 4 wt % PP composition, which would indicate, of course, the existence of either a critical point or an azeotrope[26] if simple binary polymer−solvent systems were under investigation.

Table 2 presents the experimental results obtained for the system PP−1-butene. Figure 5 displays the *P*−*x* diagram (L to LL separations). Flat boundary lines with respect to composition can be observed once more. It must be noted that VL phase behavior can only be observed when PP compositions are lower than 0.99 wt %. Besides, the crystallization boundary (L to SL, where S is solid) is intersected at higher temperatures (around 90 °C), when compared to the PP−*n*-butane system

Table 3. Experimental Results for the PP−Propane System

polym wt %	*T* [°C]	*P* [bar]	equilibrium type	polym wt %	*T* [°C]	*P* [bar]	equilibrium type
0.30	130	252.4	LL	7.48	130	263.4	LL
	125	243.0	LL		125	254.6	LL
	120	234.1	LL		120	247.1	LL
	115	224.9	LL		115	237.1	LL
	110	216.7	LL		110	228.9	LL
	105	207.9	LL		105	220.2	LL
	100	199.7	LL		100	211.0	LL
	95	190.8	LL → S		95	202.5	LL → S
1.00	130	263.7	LL	10.00	130	259.4	LL
	125	255.3	LL		125	251.1	LL
	120	246.3	LL		120	242.7	LL
	115	237.2	LL		115	234.5	LL
	110	229.1	LL		110	225.0	LL
	105	220.1	LL		105	216.7	LL
	100	211.0	LL		100	207.1	LL
	95	202.3	LL → S		95	198.8	LL → S
4.98	130	262.7	LL				
	125	254.2	LL				
	120	246.0	LL				
	115	236.9	LL				
	110	227.9	LL				
	105	219.3	LL				
	100	210.5	LL				
	95	202.4	LL → S				

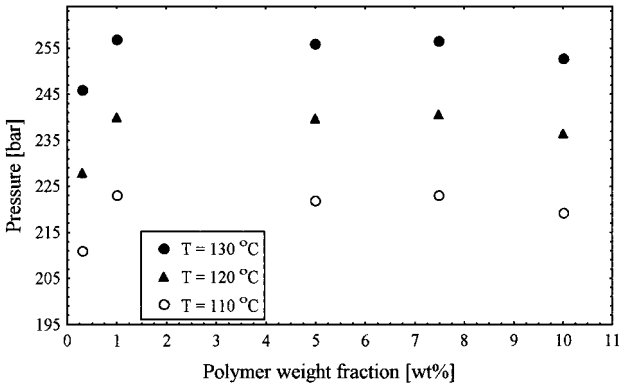

Figure 6. Experimental PP cloud-point behavior in propane. Transition from L to LL. *P*−*x* diagram.

Table 4. Experimental Results for the PP−Propylene System

polym wt %	*T* [°C]	*P* [bar]	equilibrium type	polym wt %	*T* [°C]	*P* [bar]	equilibrium type
0.30	115	253.7	LL	4.97	110	266.4	LL
	110	245.0	LL		105	257.6	LL
	105	236.4	LL		100	248.5	LL
	100	228.5	LL		95	240.6	LL → S
	95	220.7	LL → S	7.40	110	259.1	LL
0.99	110	261.0	LL		105	250.7	LL
	105	253.1	LL		100	242.3	LL
	100	242.9	LL		95	232.6	LL → S
	95	234.4	LL → S	9.84	110	257.5	LL
2.97	110	267.2	LL		105	248.3	LL
	105	258.7	LL		100	240.1	LL
	100	249.4	LL		95	231.2	LL → S
	95	240.7	LL → S				

(around 85 °C). The critical composition obtained from Figure 5 lies approximately within the range of 3−7.5 wt %.

Table 3 and Figure 6 show the experimental cloud points for the PP−propane system, while Table 4 and Figure 7 present the results for the PP−propylene system. These experimental data are in good qualitative agreement with the ones presented previously by Whaley et al.[20] for the PP−propane system, for polymer

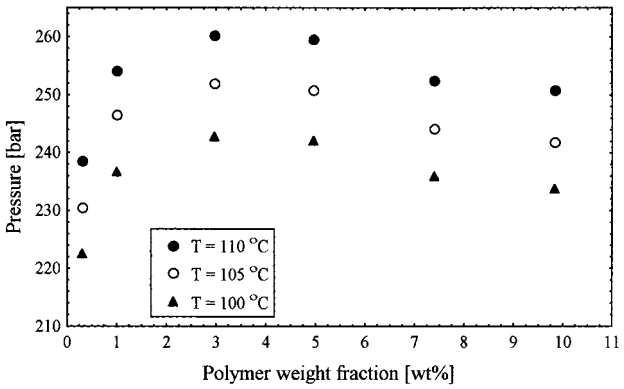

Figure 7. Experimental PP cloud-point behavior in propylene. Transition from L to LL. *P*−*x* diagram.

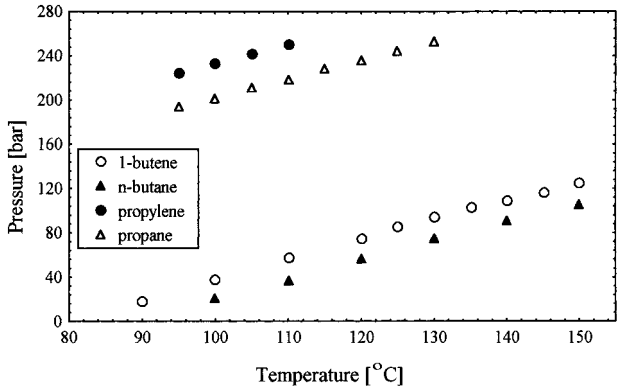

Figure 8. Comparison among L to LL cloud points for PP−hydrocarbon systems. *P*−*T* diagram at a polymer weight fraction of 10 wt %.

samples of similar molecular weight and polydispersity. For these systems, the cloud-point pressures are significantly higher than the ones obtained previously for the C4 solvents. For both systems (PP−propane and PP−propylene), solid transition temperatures increase to about 95 °C, which causes reduction of the one-phase region. For PP−propane solutions, a flat behavior is found once more when phase transitions are analyzed in the *P*−*x* diagram (Figure 6); however, for PP−propylene solutions, this behavior has not been verified. The critical concentration is approximately equal to 3 wt % for the PP−propylene system, as depicted in Figure 7.

L to LL phase transitions observed for the four PP−solvent systems analyzed previously can be compared to each other in the P−T diagrams of Figure 8, obtained for polymer compositions of around 10 wt %. The two main effects become evident. First, the chain length of the solvent affects significantly the phase behavior of the system. When C4 solvents are employed, one-phase regions are much larger than the ones obtained with the C3 solvents. Second, olefins increase cloud-point pressures and enlarge the two-phase region, when compared to alkanes with the same chain length.

Effects caused by the addition of a cosolvent were also investigated for C4 solvents. Tables 5 and 6 show the results obtained for PP−toluene−*n*-butane and PP−toluene−1-butene systems, respectively. The *P*−*T* diagrams are presented in Figures 9 and 10. The polymer concentration was kept constant at 10 wt % in order to isolate the effect of the binary solvent mixture composition upon the phase behavior. One can observe in Figures 9 and 10 that cloud-point pressures decrease

Table 5. Experimental Results for the Ternary System PP−Toluene−*n*-Butane

polym wt %	toluene wt %	*T* [°C]	*P* [bar]	equilibrium type
9.96	0.99	150	108.4	LL
		140	92.3	LL
		130	75.3	LL
		120	56.4	LL
		110	36.9	LL
		100	18.1	VL
		95	15.9	VL
		90	14.5	VL
		85	12.9	VL → S
9.83	5.09	150	99.0	LL
		140	84.1	LL
		130	66.9	LL
		120	49.1	LL
		110	30.8	LL
		100	17.5	VL
		95	15.8	VL
		90	14.3	VL
		85	12.6	VL
9.92	9.96	150	87.2	LL
		140	68.8	LL
		130	51.5	LL
		120	33.2	LL
		110	19.9	VL
		100	16.0	VL
		95	15.0	VL
		90	13.9	VL
		85	12.0	VL
		80	10.7	VL → S

Table 6. Experimental Results for the Ternary System PP−Toluene−1-Butene

polym wt %	toluene wt %	*T* [°C]	*P* [bar]	equilibrium type
9.86	1.04	150	127.5	LL
		140	111.0	LL
		130	95.4	LL
		120	75.2	LL
		110	56.6	LL
		100	35.6	LL
		95	26.3	LL
		90	17.0	VL
9.74	5.14	150	117.7	LL
		140	97.2	LL
		130	78.8	LL
		120	60.6	LL
		110	41.6	LL
		100	21.0	LL
		95	17.5	VL
		90	15.3	VL
		85	12.9	VL → S
9.93	9.85	150	102.8	LL
		140	82.6	LL
		130	66.4	LL
		120	46.2	LL
		110	26.5	LL
		100	18.3	VL
		95	16.2	VL
		90	14.0	VL
		85	11.8	VL

for both systems as the toluene content is increased. This fact may be explained in terms of the enhancement of the so-called solvent power of the solvent mixture, as the toluene content is increased. As a consequence, the region of L to LL phase transition is reduced, while the temperature range where L to VL transitions are observed increases. For example, in Figure 10, when no toluene is added to the solution, the system exhibits only L to LL phase separation. When toluene is present, transitions from L to VL are also observed. Accordingly, the LCEP is shifted to higher temperatures as the toluene content is increased in the solution.

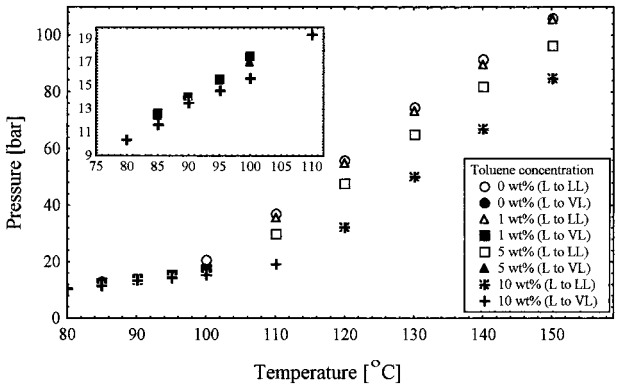

Figure 9. *P*−*T* diagram for the ternary system PP−toluene−*n*-butane at a polymer concentration of 10 wt %.

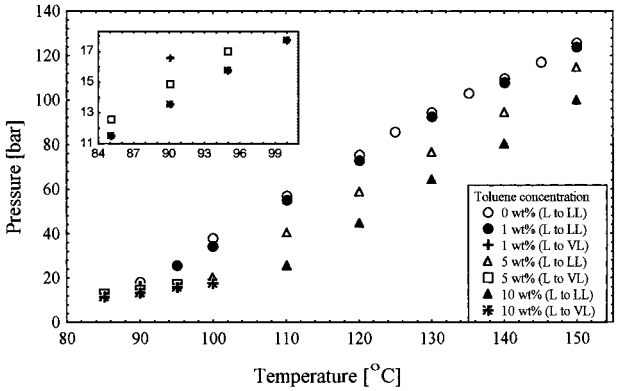

Figure 10. *P*−*T* diagram for the ternary system PP−toluene−1-butene at a polymer concentration of 10 wt %.

Enlarged views of L to VL phase transitions are depicted in Figures 9 and 10. It can be observed that cloud-point pressures decrease as the toluene content is increased. This is mainly due to the lower vapor pressure of toluene, when compared to the vapor pressures of the C4 solvents. Another effect observed experimentally is that the crystallization boundary temperature also decreases about 5 °C when toluene is added to the solution, because of the higher solvent power of the toluene solutions.

Conclusions

High-pressure phase equilibrium data for PP−propane, PP−propylene, PP−*n*-butane, and PP−1-butene are provided. Phase transitions were observed visually as cloud points and are reported for L to VL, L to LL, and LL to VLL, allowing the construction of the LCST curves for all systems and the determination of the LCEPs. When compared to olefins with the same chain length, the use of paraffins led to a decrease of cloud-point pressures, causing the increase of the one-phase region. For ternary systems containing toluene as the cosolvent, two-phase regions in the *P*−*T* diagram are reduced and cloud-point curves are shifted toward lower pressures, as the toluene content is increased. These experimental data may be of relevance for studies regarding the particle formation with controlled morphology.

Acknowledgment

The authors thank CNPq (Conselho Nacional de Desenvolvimento Científico e Tecnológico) and FAPERJ (Fundação de Apoio à Pesquisa do Estado do Rio de Janeiro) for financial support and for providing scholarships. The authors also thank Polibrasil Resinas S.A. for kindly providing the PP samples.

Literature Cited

(1) Souza, M. E.; Lima, E. L.; Pinto, J. C. A Survey on Advanced Control of Polymerization Reactors. *Polym. Eng. Sci.* **1996**, *36*, 433−447.

(2) Cavalcanti, M. J. R.; Pinto, J. C. Modeling and Optimization of Suspension SAN Polymerization Reactors. *J. Appl. Polym. Sci.* **1997**, *65* (9), 1683−1701.

(3) Sayer, C.; Lima, E. L.; Pinto, J. C.; Arzamendi, G.; Asua, J. M. MWD in Composition Controlled Emulsion Copolymerization. *Polym. React. Eng.* **1999**, submitted for publication.

(4) Canelas, D. A.; Betts, D. E.; DeSimone, J. M. Dispersion Polymerization in Supercritical Carbon Dioxide: Importance of Effective Surfactants. *Macromolecules* **1996**, *29*, 2818−2821.

(5) Lepilleur, C.; Beckman, E. J. Dispersion Polymerization of Methyl Methacrylate in Supercritical CO_2. *Macromolecules* **1997**, *30*, 745−756.

(6) Hsiao, Y. L.; Maury, E. E.; DeSimone, J. M.; Mawson, S.; Johnston, K. P. Polymerization of Methyl Methacrylate Stabilized with Poly(1,1-dihydroperfluorooctyl acrylate) in Supercritical Carbon Dioxide. *Macromolecules* **1995**, *28*, 8159−8166.

(7) Srinivasan, G.; Elliot, J. R. Microcellular Materials via Polymerization in Supercritical Fluids. *Ind. Eng. Chem. Res.* **1992**, *31*, 1414−1417.

(8) Dixon, D. J. Formation of Polymeric Materials by Precipitation with a Compressed Fluid Antisolvent. Ph.D. Thesis, The University of Texas at Austin, Austin, TX, 1992.

(9) Kontogeorgis, G. M.; Saraiva, A.; Fredenslund, A.; Tassios, D. Prediction of Liquid−Liquid Equilibrium for Binary Polymer Solutions with Simple Activity Coefficient Models. *Ind. Eng. Chem. Res.* **1995**, *34*, 1823−1834.

(10) Mawson, S.; Johnston, K. P.; Combes, J. R.; DeSimone, J. M. Formation of Poly(1,1,2,2-tetrahydroperfluorodecyl acrylate) Submicron Fibers and Particles from Supercritical Carbon Dioxide Solutions. *Macromolecules* **1995**, *28*, 3182−3191.

(11) Folie, B.; Radosz, M. Phase Equilibria in High-Pressure Polyethylene Technology. *Ind. Eng. Chem. Res.* **1995**, *34*, 1501−1516.

(12) Seckner, A. J.; McClellan, A. K.; McHugh, M. A. High-Pressure Solution Behavior of the Polystyrene−Toluene−Ethane System. *AIChE J.* **1988**, *34* (1), 9−16.

(13) Moore, E. P., Jr.; Larson, G. A. *Introduction to PP in Business* in *Polypropylene Handbook*; Moore, E. P., Jr., Ed.; Hanser Publishers: Cincinnati, OH, 1996.

(14) Kristi, L. A.; Stein, F. P.; Han, S. J.; Gregg, C. J.; Radosz, M. Phase Equilibria of Saturated and Unsaturated Polyisoprene in Sub- and Supercritical Ethane, Ethylene, Propane, Propylene, and Dimethyl Ether. *Fluid Phase Equilib.* **1996**, *117*, 84−91.

(15) Xiong, Y.; Kiran, E. Comparison of Sanchez−Lacombe and SAFT model in Predicting Solubility of Polyethylene in High-Pressure Fluids. *J. Appl. Polym. Sci.* **1995**, *55*, 1805−1818.

(16) Chen, S. J.; Radosz, M. Density-Tuned Polyolefin Phase Equilibria. I. Binary Solutions of Alternating Poly(ethylene−propylene) in Subcritical and Supercritical Propylene, 1-Butene, and 1-Hexene. Experiment and Flory−Patterson Model. *Macromolecules* **1992**, *25*, 3089−3096.

(17) Chen, S. J.; Economou, I. G.; Radosz, M. Density-Tuned Polyolefin Phase Equilibria. II. Multicomponent Solutions of Alternating Poly(ethylene−propylene) in Subcritical and Supercritical Olefins. Experiment and SAFT Model. *Macromolecules* **1992**, *25*, 4987−4994.

(18) Gregg, C. J.; Stein, F. P.; Radosz, M. Phase Behavior of Telechelic Polyisobutylene in Subcritical and Supercritical Fluids. 1. *Macromolecules* **1994**, *27*, 4972−4980.

(19) Gregg, C. J.; Stein, F. P.; Radosz, M. Phase Behavior of Telechelic Polyisobutylene in Subcritical and Supercritical Fluids. 2. *Macromolecules* **1994**, *27*, 4981−4990.

(20) Whaley, P. D.; Winter, H. H.; Ehrlich, P. Phase Equilibria of Polypropylene with Compressed Propane and Related Systems. 1. Isotactic and Atactic Polypropylene with Propane and Propylene. *Macromolecules* **1997**, *30*, 4882−4886.

(21) Dariva, C.; Stuart, G. R.; Oliveira, J. V. High-Pressure Vapor−Liquid Equilibrium for CO_2−Orange Peel Oil. *Braz. J. Chem. Eng.* **1999**, submitted for publication.

(22) Chang, J. C.; Day, C. Y.; Ko, C. M.; Chiu, K. L. Densities and $P-x-y$ Diagrams for Carbon Dioxide Dissolution in Methanol, Ethanol, and Acetone Mixtures. *Fluid Phase Equilib.* **1997**, *131*, 243−258.

(23) Suzuki, K.; Sue, H.; Itou, M.; Smith, L. R.; Inomata, H.; Arai, K.; Saito, S. Isothermal Vapor−Liquid Equilibrium Data for Binary Systems at High Pressures: Carbon Dioxide−Methanol, Carbon Dioxide−Ethanol, Carbon Dioxide−l-Propanol, Methane−Ethanol, Methane−l-Propanol, Ethane−Ethanol, and Ethane−l-Propanol Systems. *J. Chem. Eng. Data* **1990**, *35*, 63−66.

(24) Day, C. Y.; Chang, J. C.; Chen, C. Y. Phase Equilibrium of Ethanol + CO_2 and Acetone + CO_2 at Elevated Pressures. *J. Chem. Eng. Data* **1996**, *41*, 839−843.

(25) Haschets, C. W.; Shine, A. D. Phase Behavior of Polymer−Supercritical Chlorodifluoromethane Solutions. *Macromolecules* **1993**, *26*, 5052−5060.

(26) Rowlison, J. S.; Swinton, F. L. *Liquids and Liquid Mixtures*; Butterworth Scientific: London, 1982.

Received for review December 15, 1999
Revised manuscript received July 17, 2000
Accepted July 20, 2000

IE990895S